

Article

# Building Earthquake Damage Information Extraction from a Single Post-Earthquake PolSAR Image

Wei Zhai <sup>1,2,3,4</sup>, Huanfeng Shen <sup>5</sup>, Chunlin Huang <sup>2,4,\*</sup> and Wansheng Pei <sup>6</sup>

<sup>1</sup> Gansu Earthquake Administration, Lanzhou 730000, China; zwxxxxdsyhq@163.com

<sup>2</sup> Key Laboratory of Remote Sensing of Gansu Province, Cold and Arid Regions Environmental and Engineering Research Institute, Chinese Academy of Sciences, Lanzhou 730000, China

<sup>3</sup> College of Resources and Environment, University of Chinese Academy of Sciences, Beijing 100049, China

<sup>4</sup> Heihe Remote Sensing Experimental Research Station, Cold and Arid Regions Environmental and Engineering Research Institute, Chinese Academy of Sciences, Lanzhou 730000, China

<sup>5</sup> School of Resource and Environmental Sciences, Wuhan University, Wuhan 430079, China; shenhf@whu.edu.cn

<sup>6</sup> Cold and Arid Regions Environmental and Engineering Research Institute, Chinese Academy of Sciences, Lanzhou 730000, China; peiwansheng@126.com

\* Correspondence: huangcl@lzb.ac.cn; Tel.: +86-0931-496-7975

Academic Editors: Zhenhong Li, Roberto Tomas, Zhong Lu and Prasad S. Thenkabail

Received: 25 November 2015; Accepted: 16 February 2016; Published: 25 February 2016

**Abstract:** After an earthquake, rapidly and accurately obtaining building damage information can help to effectively guide the implementation of the emergency rescue and can reduce disaster losses and casualties. Using a single post-earthquake fully-polarimetric synthetic aperture radar (PolSAR) image to interpret building damage information not only involves a guaranteed data source but is also easy and can be rapidly implemented. This paper is focused on rapid building earthquake damage detection in urban areas using post-earthquake PolSAR data. In PolSAR images, the undamaged buildings parallel to satellite flight pass are different from the collapsed buildings, but the undamaged buildings divergent to satellite flight pass are very similar to collapsed buildings because of their volume scattering characteristics. In this paper, the method of polarization orientation angle (POA) compensation is employed to increase the scattering power of buildings divergent to satellite flight pass, and then Wishart supervised classification is implemented on the PolSAR data after POA compensation. In addition, the two parameters of normalized difference of the dihedral component (NDDC) and  $\rho_{HHHV}$  are proposed to improve the classification accuracy of the Wishart supervised classification, and both the undamaged buildings and collapsed buildings are determined. The study was carried out after the “4.14” Yushu earthquake in Yushu County, Qinghai province, China. The three damage levels are set for the urban area at the city block scale according to the values of the *BBCR* building damage index. The experimental results confirm that the scheme proposed in this paper can greatly improve the accuracy of the extraction of building damage information.

**Keywords:** earthquake; buildings; damage assessment; PolSAR

## 1. Introduction

In recent years, earthquake disasters have become more frequent around the world. The earthquake is one of the most dangerous natural disasters for human beings, and tens of billions of dollars in property loss are caused by earthquakes every year. Unfortunately, earthquakes cannot be predicted accurately at the current scientific level. Rapid and accurate damage assessment can help to reduce the disaster loss and can provide decision support for the rescue and reconstruction efforts. Buildings are

the places where people live, and most of the casualties and economic losses in an earthquake are caused by the damage to buildings [1]. Therefore, building damage assessment is one of the most important parts of earthquake damage assessment.

The earthquake damage information obtained from a ground survey is the most accurate, but this process is inefficient and takes a long period of time. Remote sensing, which is characterized by wide coverage and speediness, is very suitable for areas with poor transport infrastructure and where there is a risk of secondary disasters. Optical remote sensing images allow easy interpretation, but they are susceptible to illumination variation [2]. Radar, with its strong penetrating ability, can operate day and night, independent of weather conditions. As a result, radar has become an important means of disaster assessment [3–6], but most of the studies of disaster assessment are based on multi-source [7,8] or multi-temporal data [9–12]. However, obtaining the matched pre-earthquake data is difficult in some situations, and the registration of the pre- and post-earthquake data is tricky and time-consuming. Therefore, it is quicker and more convenient to undertake earthquake damage assessment using only post-event single-temporal data.

Balz [13], Dell'Acqua *et al.* [14], and Polli *et al.* [15] have all evaluated building earthquake damage using only post-earthquake single-polarization synthetic aperture radar (SAR) data. Nevertheless, PolSAR (fully-polarimetric SAR) data record the scattering amplitude and phase of the HH (horizontal/horizontal polarization), HV (horizontal/vertical polarization), VH (vertical/horizontal polarization), and VV (vertical/vertical polarization) polarizations four ways for ground objects, and can better assist with the understanding of scattering mechanisms [16] than single-polarization SAR imagery. As a result, building damage assessment using PolSAR imagery is more accurate and more reliable. Guo *et al.* [17] and Li *et al.* [18] introduced the parameter of  $\rho$  (circular polarization correlation coefficient) and proposed the  $H-\alpha-\rho$  method to extract the spatial distribution of collapsed buildings in the Yushu urban area by using only a single post-earthquake SAR image. Subsequently, Zhao *et al.* [19] improved the  $H-\alpha-\rho$  method and replaced the parameter of  $\rho$  with the normalized circular-pol correlation coefficient (NCCC), and, at the same time, the *homogeneity* texture feature was employed to solve the problem of collapsed buildings and buildings divergent to satellite flight pass being mixed with each other. Shen *et al.* [20] extracted collapsed buildings based on feature template matching, using 13 polarimetric features. On account of the present research into building earthquake damage information extraction being rather limited, this work aims to undertake some new research in this area.

A new scheme for earthquake damage assessment using only a single post-earthquake PolSAR image is proposed in this study. This work explores the potential of using polarimetric information to estimate earthquake damage for urban regions. In full PolSAR imagery, the scattering power of collapsed buildings characterized by volume scattering is weak, and the undamaged buildings are mainly characterized by double-bounce scattering, for which the scattering power is strong. However, the buildings divergent to satellite flight pass, which are not parallel to the flight pass, with significant cross-polarization backscattering, are similar to the collapsed buildings. This ambiguity between the building types commonly results in overestimation of collapsed buildings in damage assessment.

The buildings divergent to satellite flight pass, rather than the buildings parallel to satellite flight pass, rotate the polarization basis and induce a polarization orientation angle (POA) shift from zero [21]. Therefore, we first implement POA compensation for the original PolSAR data in order to solve the scattering mechanism ambiguity between collapsed buildings and buildings divergent to satellite flight pass. Wishart supervised classification is then performed on the PolSAR data after POA compensation to extract the initial earthquake damage information. The parameters of the normalized difference of the dihedral component (NDDC) and the HH-HV correlation coefficient ( $\rho_{HHHV}$ ) are then introduced to extract the buildings divergent to satellite flight pass, which are added to the undamaged buildings generated from the Wishart supervised classification. The  $\rho_{HHHV}$  parameter is also used to improve the vegetation classification result of the Wishart supervised classification. When the undamaged buildings and collapsed buildings are acquired, the building collapse rate is quantized at the block

level by the building block collapse rate (BBCR). Finally, a map with three building damage levels for the whole urban region is drawn according to the threshold value of the BBCR at the block scale.

## 2. Methodology

### 2.1. The Damage Assessment Procedures

There are five key procedures in the process flow of the damage estimation framework proposed in this study, as shown in Figure 1. Firstly, according to Section 2.2, the method of POA compensation is performed using the PolSAR data after preprocessing, and the new [T3] matrix after POA compensation is obtained.

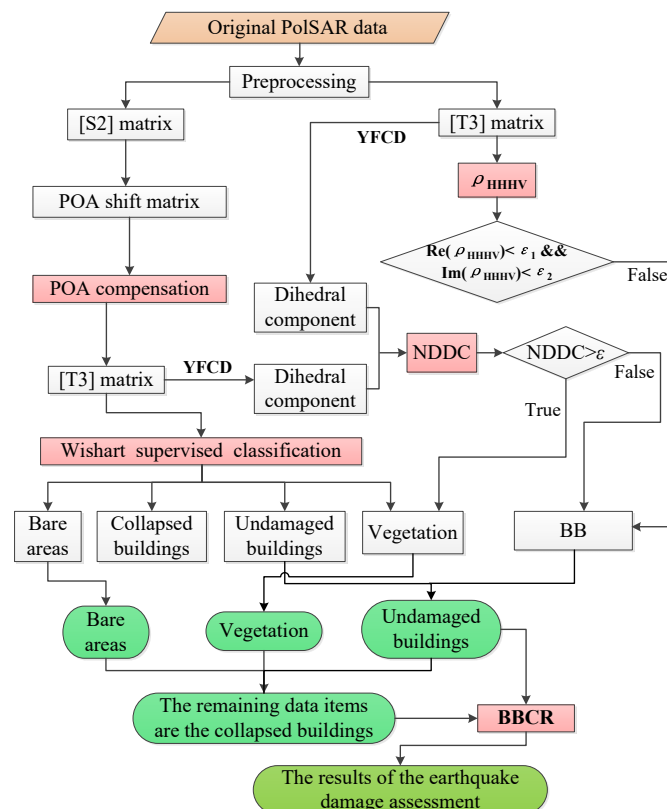


**Figure 1.** The process flow diagram of the damage estimation framework. “YFCD”, “BB”, “Re” and “Im” represent the Yamaguchi four-component decomposition, the buildings divergent to satellite flight pass, and the real part and imaginary part of the complex number, respectively.  $\epsilon$ ,  $\epsilon_1$ , and  $\epsilon_2$  are the threshold values.

Secondly, the Wishart supervised classification is performed on the PolSAR data after POA compensation, and this procedure classifies the ground objects into the four classes of undamaged buildings, collapsed buildings, vegetation, and bare areas.

Thirdly, Yamaguchi four-component decomposition is performed on the PolSAR data before and after POA compensation, respectively. At the same time, the two dihedral components are respectively extracted to compute the NDDC, as described in Section 2.4. Next, the  $\rho_{HHHV}$  parameter described in Section 2.4 is computed. The buildings divergent to satellite flight pass are then extracted using the two parameters of the NDDC and  $\rho_{HHHV}$ . The data items of buildings divergent to satellite flight pass are added to the undamaged buildings generated from the Wishart supervised classification, and they become the total undamaged buildings.

According to the third step, the undamaged buildings are extracted. The collapsed buildings are extracted in the fourth step. The vegetation class generated from the Wishart supervised classification

is corrected by meeting the condition of  $NDDC < \varepsilon$ . The final output of the class of bare areas is the same as the classification result of the Wishart supervised classification. After the three classes of undamaged buildings, vegetation, and bare areas are determined, the remaining data items are the collapsed buildings.

Finally, the building collapse rate of each block is derived from the BBCR index described in Section 2.6, and the damage levels of all the blocks are divided into three levels according to the threshold values of the BBCR index. The earthquake damage assessment with three damage levels is then mapped out for the whole urban region. The methodology and parameters are introduced in detail in the next section.

## 2.2. Polarization Orientation Angle (POA) Compensation

For enhancing the contrast between buildings divergent to satellite flight pass and collapsed buildings, the scheme of POA compensation can be used to increase the double-bounce scattering power of buildings divergent to satellite flight pass.

The buildings divergent to satellite flight pass patch can induce the POA shift  $\theta$ , which can be estimated by Equation (1) based on the circular polarization method [21,22]:

$$\theta = \begin{cases} \theta_0, & \text{if } \theta_0 \leq \frac{\pi}{4} \\ \theta_0 - \frac{\pi}{2}, & \text{if } \theta_0 > \frac{\pi}{4} \end{cases} \quad (1)$$

where

$$\theta_0 = \frac{1}{4} [Arg(\langle S_{RR} S_{LL}^* \rangle) + \pi] \quad (2)$$

According to Lee [21], the data compensation of the orientation angle of  $\theta$  can be achieved by:

$$T_\theta = R(\theta) TR(\theta)^T \quad (3)$$

where the superscript  $T$  denotes the matrix transpose, and the rotation matrix  $R(\theta)$  is given by:

$$R(\theta) = \begin{bmatrix} 1 & 0 & 0 \\ 0 & \cos 2\theta & \sin 2\theta \\ 0 & -\sin 2\theta & \cos 2\theta \end{bmatrix} \quad (4)$$

## 2.3. Wishart Supervised Classification

The scattering power of PolSAR imagery can be greatly increased using the method of POA compensation. Therefore, in order to extract the undamaged buildings as completely as possible, Wishart supervised classification based on the complex Wishart distribution of the polarimetric coherency matrix [23] is performed on the PolSAR data after POA compensation. The classification algorithm proposed in [24] for polarimetric SAR images is the recommended method for supervised classification. Details of the Wishart supervised classification algorithm can be found in [23]. The ground objects are classified into four categories using the Wishart supervised classification: undamaged buildings, collapsed buildings, vegetation, and bare areas. Among the classification results, the buildings divergent to satellite flight pass will be mixed in both the collapsed buildings and vegetation classes, so the two classes obtained from the Wishart supervised classification will be inaccurate. The undamaged buildings class still lack some of the buildings divergent to satellite flight pass whose scattering power is not strong enough. However, the bare areas class has a high reliability. Therefore, the results of the Wishart supervised classification are considered as the initial classification results for extracting the building damage information. The initial extraction results are then improved using the following two indicators.

#### 2.4. Building Divergent to Satellite Flight Extraction

Because the results of the Wishart supervised classification are not very accurate, the two parameters of the NDDC and  $\rho_{HHHV}$  are proposed to correct the initial classification results. The buildings divergent to satellite flight pass are extracted using the two parameters of the NDDC and  $\rho_{HHHV}$ , which are introduced in the following.

The indicator of the difference of the dihedral component (DDC) is defined as the difference between the dihedral component obtained from the Yamaguchi four-component decomposition [25,26] before and after POA compensation. It can be expressed as: the DDC equals the dihedral component after POA compensation minus the dihedral component before POA compensation. The DDC is normalized to a positive value range, which is named the normalized difference of the dihedral component, or the NDDC for short.

The scattering power of the buildings divergent to satellite flight pass is greatly increased after the POA compensation. Meanwhile, the scattering intensity of the dihedral component generated from the Yamaguchi four-component decomposition is also increased. The NDDC can measure the change in the double-bounce scattering power after the POA compensation. The double-bounce scattering power of the buildings divergent to satellite flight pass changes a great deal after the POA compensation, while that of the targets with reflection symmetry changes little. That is, the NDDC values of the buildings divergent to satellite flight pass are high and those of the targets with reflection symmetry are low. Hence, the NDDC can be introduced in the process of earthquake damage assessment to find the buildings divergent to satellite flight pass, which can be used to correct the classification result of the undamaged buildings generated from the Wishart supervised classification. The scattering intensity of some buildings divergent to satellite flight pass is not increased to as strong as the buildings parallel to satellite flight pass using the method of POA compensation. Therefore, the class of undamaged buildings obtained from the Wishart supervised classification is not complete. The main missing undamaged buildings are the buildings divergent to satellite flight pass whose scattering intensity is not significantly increased. The data items with high NDDC values correspond to the buildings divergent to satellite flight pass, which can be added to the undamaged buildings. The threshold value  $\varepsilon$  of the NDDC is set to distinguish the buildings divergent to satellite flight pass from the other ground objects:

$$x \in \text{buildings divergent to satellite flight pass, if } \text{NDDC}(x) > \varepsilon \quad (5)$$

The  $\rho_{HHHV}$  parameter is computed using the following equation:

$$\rho_{HHHV} = \frac{\langle S_{HH}S_{HV}^* \rangle}{\sqrt{\langle S_{HH}S_{HH}^* \rangle} \sqrt{\langle S_{HV}S_{HV}^* \rangle}} \quad (6)$$

where the superscript \* denotes the complex conjugate.

In our experiments, we found that the distributions in the complex plane of the  $\rho_{HHHV}$  parameter for the buildings divergent to satellite flight pass and collapsed buildings are different. The  $\rho_{HHHV}$  parameter for the collapsed buildings is mainly distributed in the third quadrant of the complex plane, while the  $\rho_{HHHV}$  parameter for the buildings divergent to satellite flight pass is mainly distributed in the other areas of the complex plane. Therefore, the buildings divergent to satellite flight pass can be extracted using the  $\rho_{HHHV}$  parameter by the expression:

$$x \in \text{buildings divergent to satellite flight pass,} \\ \text{if } (\text{Re}(\rho_{HHHV}(x)) < \varepsilon_1 \ \& \ \text{Im}(\rho_{HHHV}(x)) < \varepsilon_2) = 0 \quad (7)$$

where  $x$  is the data sample of the PolSAR imagery; “Re” and “Im” denote the real part and imaginary part of the complex number, respectively; and  $\varepsilon_1$  and  $\varepsilon_2$  are the two threshold values of the real part and imaginary part of  $\rho_{HHHV}$ , respectively.

The  $\rho_{HHHV}$  parameter is computed using the PolSAR data without POA compensation, which can better distinguish collapsed buildings from buildings divergent to satellite flight pass than using the PolSAR data after POA compensation, based on experiments.

In this work, the parameters of  $\rho_{HHHV}$  and the NDDC together determine the buildings divergent to satellite flight pass. The buildings divergent to satellite flight pass extracted using the NDDC include some collapsed buildings with the walls divergent to satellite flight, but the buildings divergent to satellite flight pass extracted by the  $\rho_{HHHV}$  parameter contain a few collapsed buildings with the walls divergent to satellite flight. Therefore, the data items simultaneously satisfying the two conditions of  $\rho_{HHHV}$  and the NDDC are determined as the buildings divergent to satellite flight pass, which can result in a higher extraction accuracy for the buildings divergent to satellite flight pass. Using the parameters of  $\rho_{HHHV}$  and the NDDC to extract the buildings divergent to satellite flight pass can be expressed as:

$$\begin{aligned} &x \in \text{buildings divergent to satellite flight pass,} \\ &\text{if } \text{NDDC}(x) > \varepsilon \ \& \ (\text{Re}(\rho_{HHHV}(x)) < \varepsilon_1 \ \& \ \text{Im}(\rho_{HHHV}(x)) < \varepsilon_2) = 0 \end{aligned} \quad (8)$$

The buildings divergent to satellite flight pass extracted by the parameters of  $\rho_{HHHV}$  and the NDDC, together with the undamaged buildings generated from the Wishart supervised classification, are the final output undamaged buildings.

### 2.5. Collapsed Building Extraction

The vegetation class generated from the Wishart supervised classification still needs to be corrected. The NDDC values of vegetation items with reflection symmetry are low, and this property can be used to correct the classification result of the Wishart supervised classification for the vegetation class. Therefore, the data items of the vegetation generated from the Wishart supervised classification should simultaneously satisfy the condition of  $\text{NDDC} < \varepsilon$ , and can be determined as the final output of the vegetation class. The buildings divergent to satellite flight pass are determined according to Section 2.4, and the bare areas are obtained through the Wishart supervised classification. By excluding the data items of the above three classes, the remaining data items can be classified as the collapsed buildings.

### 2.6. Building Collapse Rate Calculation

The building collapse rate is calculated at the block scale, and is defined as the ratio of the collapsed building samples to the total number of building samples in one block. The damage level of one block can be indexed by the building collapse rate of the block. The building collapse rate of blocks is introduced to handle the damage assessment at the block scale, and it is termed the building block collapse rate (BBCR). The blocks separated by roads are regarded as individual areas of similar built-up patch structure [19]. Each block is assigned a BBCR to assess the damage level of the block. The BBCR is expressed as:

$$\text{BBCR}_j = \frac{\sum_i C_{ij}}{\sum_i U_{ij} + \sum_i C_{ij}} \quad (9)$$

where  $\text{BBCR}_j$  is the BBCR of the  $j$ th block;  $C_{ij}$  indicates whether pixel  $i$  in the  $j$ th block belongs to a collapsed building or not, with values of 0 or 1; and  $U_{ij}$  indicates whether pixel  $i$  in the  $j$ th block belongs to an undamaged building or not, with values of 0 or 1.

## 3. Experimental Results and Analysis

### 3.1. Experimental Data

The study case is the “4.14” Yushu earthquake with magnitude 7.1 which occurred on 14th April, 2010. This earthquake severely affected the county of Yushu in Qinghai province of China. The location of the

epicenter was 33.1°N and 96.6°E, as shown in Figure 2. The area is characterized by complicated terrain, poor transport infrastructure, and harsh climate. The vegetation of the Yushu urban region is sparse and low level, and the buildings are mainly rural residential buildings. More than 240,000 people were affected by the earthquake, and more than 2600 people died as a result of the earthquake. There were many collapsed buildings and more than 22 billion CNY of direct economic losses. The experiments were carried out on the post-event airborne PolSAR imagery to validate the effectiveness of the proposed approach for earthquake damage assessment. The PolSAR imagery was acquired one day after the earthquake by the Chinese airborne SAR mapping system (SARMapper), which was developed by a group led by the Chinese Academy of Surveying and Mapping (CASM). The system collects P-band data, and both the range resolution and azimuth resolution are approximately 1 m. Some specific information about the PolSAR data used in this work is listed in Table 1. The Pauli RGB image is shown in Figure 3, formed as a color composite of  $|HH - VV|$  (red),  $|HV|$  (green), and  $|HH + VV|$  (blue), with the size of 8192 × 4384 pixels. The mountains surrounding Yushu County account for a large part of the imagery. In order to focus on analyzing the buildings of the urban area, an urban area mask was applied to discard the mountains and preserve the urban area as the region of interest. To allow a comparison with the existing damage assessment maps of the 4.14 Yushu earthquake [19,27,28], the geographic information system (GIS) data layer was depicted manually along the major roads and by reference to these damage assessment maps. The urban area was divided into 72 blocks by the GIS data layer containing 72 polygons, and the layout and characteristics of the buildings within the city blocks were similar. The ground-truth map shown in Figure 4 was drawn with reference to the above-mentioned damage assessment maps [19,27,28] and the high-resolution QuickBird image of Yushu County, and the damage levels were grouped into three levels for the 72 city blocks.

**Table 1.** Information about the fully-polarimetric synthetic aperture radar (PolSAR) data used in this work.

Date	Flight Direction	Illumination Direction	Incidence Angle	Band	Flight Altitude (m)	Spatial Resolution (m)
15 April 2010	From right to left	Bottom	50°	P	10,079	1 (range); 1 (azimuth)

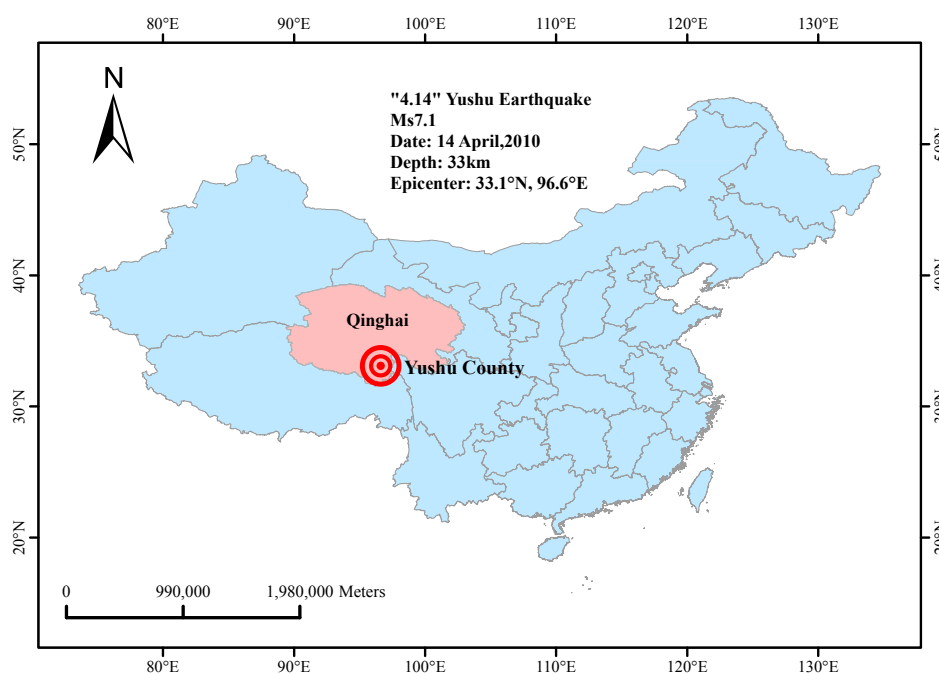


**Figure 2.** Map of the location of Yushu earthquake.

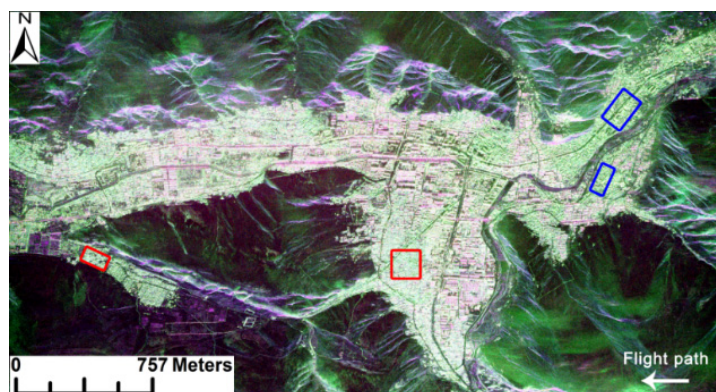


**Figure 3.** Pauli RGB color composite ( $|HH - VV|$  (red),  $|HV|$  (green), and  $|HH + VV|$  (blue)) image of Yushu County. The areas marked by red and blue rectangles are the samples for collapsed buildings and buildings divergent to satellite flight pass, respectively. The center coordinates of the image are  $33^{\circ}0'9''N$  and  $97^{\circ}0'11''E$ .

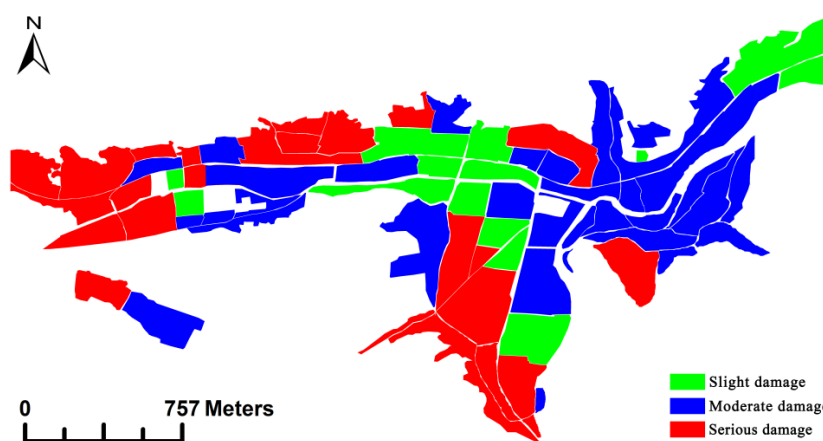


**Figure 4.** Reference map for the earthquake damage assessment, with three damage levels: slight damage, moderate damage, and serious damage. If more than half of the buildings collapsed after the earthquake, the city block was considered as serious damage. The city block with less than one-third buildings collapsing was considered as slight damage. The city block with the damage level between slight damage and serious damage was considered as moderate damage.

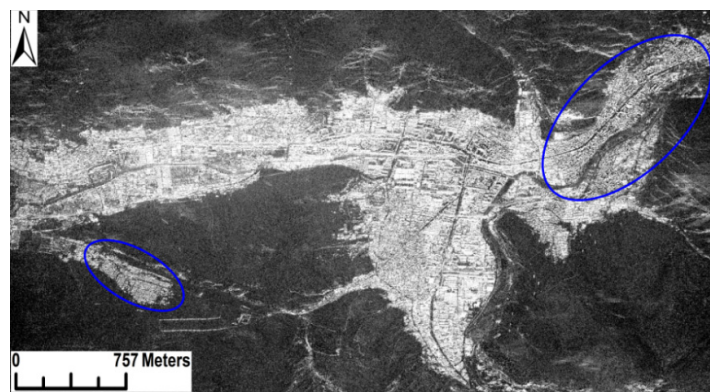
### 3.2. The Results of the Experiments

According to the process flow of the earthquake damage assessment shown in Figure 1, the POA shift was first estimated based on the circular polarization method, and the POA compensation described in Section 2.2 was carried out for the PolSAR data after speckle noise filtering. The two dihedral components before and after POA compensation were then extracted on the basis of Yamaguchi four-component decomposition. As can be seen from Figure 5, the dihedral component image brightness changed after the POA compensation, and there are great differences in some parts of the two images, such as the upper right part and the bottom left part. These areas are mainly undamaged buildings divergent to satellite flight pass and collapsed buildings divergent to satellite flight pass. The NDDC parameter described in Section 2.4 was calculated and is shown in Figure 6. According to the color bar in Figure 6, 190 can be easily chosen as the threshold value for distinguishing the buildings divergent to satellite flight pass from the other ground objects, which are mainly reflection symmetric. The areas corresponding to  $NDDC > 190$  are mainly buildings divergent to satellite flight pass. Meanwhile, the PolSAR data after POA compensation were classified into undamaged buildings, collapsed buildings, vegetation, and bare areas using the Wishart supervised classification described

in Section 2.3. For vegetation, the NDDC was less than 190. Therefore, if a data item was classified as vegetation by the Wishart supervised classification, and simultaneously satisfied  $NDDC < 190$ , it was finally classified as vegetation.



(a)



(b)

**Figure 5.** Images of the dihedral component before and after POA compensation. (a) before POA compensation; (b) after POA compensation.

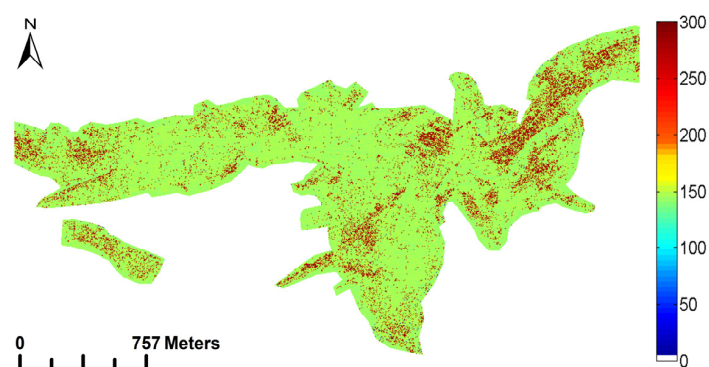


**Figure 6.** NDDC map.

The  $\rho_{HHHV}$  parameter was calculated according to Section 2.4 using the PolSAR data without POA compensation. The 5000 samples were randomly selected from the two regions of interest (ROIs) of buildings divergent to satellite flight pass and the two ROIs of collapsed buildings, respectively, and are shown in Figure 7. As can be seen from Figure 7, the collapsed building samples are mainly distributed in the third quadrant of the complex plane, and the buildings divergent to satellite flight samples are mainly located in other parts of the complex plane. Therefore, the buildings divergent to

satellite flight pass class can be finally determined by the condition that the complex number  $\rho_{HHHV}$  is not in the third quadrant of the complex plane, and the NDDC is greater than 190. The buildings divergent to satellite flight pass and the undamaged buildings generated from the Wishart supervised classification, which are mainly undamaged buildings parallel to satellite flight pass, together form the final classification result of the undamaged buildings.

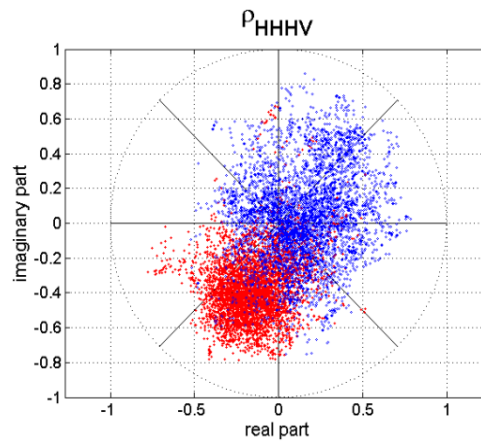


**Figure 7.**  $\rho_{HHHV}$  of the building divergent to satellite flight samples and collapsed building samples. The red dots and blue dots represent the collapsed building samples and the building divergent to satellite flight samples, respectively.

The bare areas class was determined by the classification result of the Wishart supervised classification. The collapsed buildings were considered to be the remaining parts after removing the three classes of vegetation, undamaged buildings, and bare areas. The distribution map of the non-buildings and the three kinds of buildings is shown in Figure 8. The building damage level index of each block was implemented using the BBCR method described in Section 2.6, as shown in Figure 9. A greater BBCR value corresponds to a more seriously damaged block. Three damage levels were set for the building collapse degree of the blocks. When the BBCR was less than 0.3, the damage level was set as slight damage. A BBCR of greater than 0.5 was set as the serious damage level, and a BBCR value of between 0.3 and 0.5 was considered to be moderate damage. The results of the damage assessment are shown in Figure 10, where the numbered blocks are the misclassified blocks, and the color of the numbers denotes the correct damage level. For example, the no. 8 block should actually be slightly damaged (green), but is misclassified as moderate damage (blue).

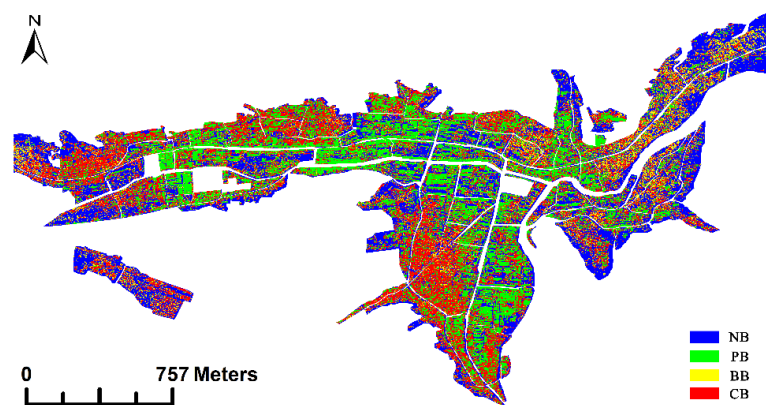


**Figure 8.** Distribution map of the non-buildings and the three kinds of buildings at the block scale. The NB, PB, BB and CB represent the non-buildings, the buildings parallel to satellite flight pass, the buildings divergent to satellite flight pass and the collapsed buildings, respectively.



Figure 9. BCCR map for each block.

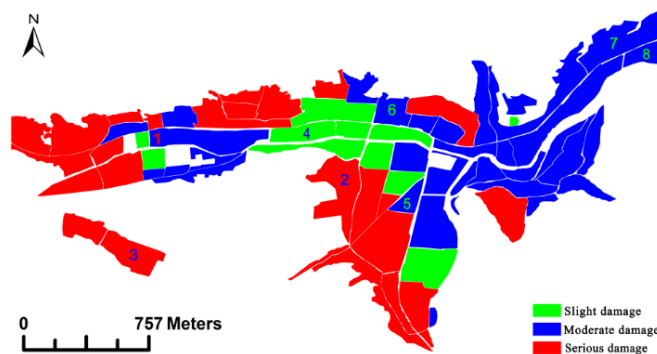


Figure 10. The damage assessment results. The numbered blocks are misclassified, and the color of the numbers denotes the color of the correct damage level.

### 3.3. Analysis and Discussion

The whole procedure of the production of a damage assessment map has taken five to six hours, which can meet rapid acquisition for buildings damage information after an earthquake. The damage assessment accuracies of the proposed method and the method only using the PolSAR data without POA compensation for the Wishart supervised classification are listed in Table 2. As can be seen in Table 2, the method proposed in this study significantly improves the damage assessment accuracy. In addition, compared with the method proposed by Zhao *et al.* [19], the proposed method again greatly improves the damage assessment accuracy. For the seriously damaged blocks, there are actually 25 blocks in the ground-truth map, but there are 31 blocks classified by the Wishart supervised classification using the PolSAR data without POA compensation, while there are 26 blocks generated by the proposed method. Therefore, the method proposed in this study also reduces the over-assessment of the building collapse rate, which could help to save human, physical, and financial resources for the emergency rescue after an earthquake.

Table 2. Comparison of the damage assessment accuracy of the two methods.

	The Proposed Method			Wishart Supervised Classification			
	(Experiment)						
	SLD	MOD	SED	SLD	MOD	SED	
	(No. of Blocks)						
(Reference)	SLD	10	4	0	9	3	2
	MOD	1	30	2	3	22	8
	SED	0	1	24	0	4	21
	OA: 88.89%			OA: 72.22%			

OA, SLD, MOD, and SED represent overall accuracy, slight damage, moderate damage, and serious damage, respectively.

For the results of the method proposed in this study with the Yushu earthquake data, there are eight blocks misclassified. Among them, the damage levels of both block no. 1 and block no. 4 are underestimated, while the damage levels of blocks no. 2 and no. 3 and blocks nos. 5 to 8 are overestimated. These blocks are mainly low-rise and small rural residential buildings with earth/wood structure or masonry structure. The remaining walls of the collapsed buildings present dihedral scattering characteristics and are easily misclassified as undamaged buildings. Thus, some remaining parts of the damaged buildings parallel to satellite flight pass and the damaged buildings divergent to satellite flight pass may be misclassified as undamaged buildings, which is the main reason for the underestimation of the block damage level. The buildings divergent to satellite flight pass cannot be completely extracted with just the two parameters of the NDDC and  $\rho_{HHHV}$ , so some ground objects with comparatively weak scattering power and characterized by volume scattering are still classified as collapsed buildings. This results in the overestimation of the building collapse rate at the block scale.

#### 4. Conclusions

Collapsed buildings caused by an earthquake are one of the main causes of casualties, so rapid acquisition of the collapsed building information after the earthquake can play an extremely important role in saving lives. The use of only a single post-earthquake PolSAR image to extract the collapse information can meet the needs of rapid and accurate disaster information acquisition, and can assist with a rapid and effective emergency rescue operation. In this study of earthquake damage assessment, the two parameters of the NDDC and  $\rho_{HHHV}$  were used to improve the classification results of Wishart supervised classification performed on the PolSAR data after POA compensation, with the aim of obtaining non-buildings, undamaged buildings (including the buildings parallel to satellite flight pass and the buildings divergent to satellite flight pass), and collapsed buildings.

This feasibility study was performed on the airborne PolSAR imagery acquired one day after the Yushu earthquake. The buildings divergent to satellite flight pass were extracted based on the conditions of  $NDDC > 190$  and  $\rho_{HHHV}$  not being in the third quadrant of the complex plane, and were included in the undamaged buildings. These operations improved the accuracy of the undamaged building extraction. Using the condition of  $NDDC < 190$  to restrict the vegetation generated from the Wishart supervised classification improved the non-building extraction accuracy and reduced the numbers of collapsed buildings divergent to satellite flight pass mixed with the vegetation class. At the same time, the above operations excluded the non-buildings and undamaged buildings as much as possible, and also improved the extraction accuracy of the collapsed buildings. Finally, the earthquake damage assessment map of the Yushu urban region with three damage levels at the block scale was obtained according to the value of the BCCR index for each block. The damage assessment at the block scale can not only be flexibly applied to multiple-resolution radar images and can avoid some of the errors of damage assessment at the single-building scale, but could also be more effective in assisting with making comprehensive arrangements in the process of emergency rescue.

All in all, the method proposed in this study can greatly improve the accuracy of earthquake damage assessment. Nevertheless, some undamaged buildings divergent to satellite flight still cannot be extracted, and some remaining parts of collapsed buildings are easily misidentified as undamaged buildings, which is the main reason for the errors in the building earthquake damage information extraction. In our future work, state-of-the-art filtering methods [29] and multi-classifier fusion [30,31] will be considered to improve the current results.

**Acknowledgments:** This work was supported by the Program for Changjiang Scholars and Innovative Research Team in University (IRT1278); the Hundred Talent Program of the Chinese Academy of Sciences (29Y127D01); the Cross-Disciplinary Collaborative Teams Program for Science, Technology and Innovation of the Chinese Academy of Sciences; the Earthquake Science and Technology Development Fund Program of Lanzhou Earthquake Research Institute, the China Earthquake Administration (2015M02); the Object-Oriented High Trusted SAR Processing System of the National 863 Subject Program; and the Airborne Multiband Polarimetric Interferometric SAR Mapping System of the National Major Surveying and Mapping Science and Technology Special Program. We would also like to thank the anonymous reviewers for their advice on improving the quality of this paper.

**Author Contributions:** Wei Zhai drafted the manuscript and was responsible for the research design, writing the source code, data analysis, and interpretation of the results. HuanfengShen designed the structures of the paper and guided the experiments. Chunlin Huang edited and reviewed the manuscript. Wansheng Pei collected literatures.

**Conflicts of Interest:** The authors declare no conflict of interest.

## References

1. Matsuoka, M.; Yamazaki, F. Use of satellite SAR intensity imagery for detecting building areas damaged due to earthquakes. *Earthq. Spectra* **2004**, *20*, 975–994. [[CrossRef](#)]
2. Zhai, W.; Shen, H.; Huang, C.; Pei, W. Fusion of polarimetric and texture information for urban building extraction from fully polarimetric SAR imagery. *Remote Sens. Lett.* **2016**, *7*, 31–40. [[CrossRef](#)]
3. Matsuoka, M.; Nojima, N. Building damage estimation by integration of seismic intensity information and satellite L-band SAR imagery. *Remote Sens.* **2010**, *2*, 2111–2126. [[CrossRef](#)]
4. Shinozuka, M.; Ghanem, R.; Houshmand, B.; Mansouri, B. Damage detection in urban areas by SAR imagery. *J. Eng. Mech.* **2000**, *126*, 769–777. [[CrossRef](#)]
5. Miura, H.; Midorikawa, S.; Matsuoka, M. Building damage assessment using high-resolution satellite SAR images of the 2010 Haiti Earthquake. *Earthq. Spectra* **2015**. [[CrossRef](#)]
6. Trianni, G.; Gamba, P. Damage detection from SAR imagery: Application to the 2003 Algeria and 2007 Peru earthquakes. *Int. J. Navig. Observ.* **2008**. [[CrossRef](#)]
7. Chini, M.; Pierdicca, N.; Emery, W.J. Exploiting SAR and VHR optical images to quantify damage caused by the 2003 Bam earthquake. *IEEE Trans. Geosci. Remote Sens.* **2009**, *47*, 145–152. [[CrossRef](#)]
8. Brunner, D.; Lemoine, G.; Bruzzone, L. Earthquake damage assessment of buildings using VHR optical and SAR imagery. *IEEE Trans. Geosci. Remote Sens.* **2010**, *48*, 2403–2420. [[CrossRef](#)]
9. Ciampalini, A.; Bardi, F.; Bianchini, S.; Frodella, W.; Ventisette, C.D.; Moretti, S.; Casagli, N. Analysis of building deformation in landslide area using multisensor PSInSAR™ technique. *Int. J. Appl. Earth Obs.* **2014**, *33*, 166–180. [[CrossRef](#)]
10. Gamba, P.; Dell’Acqua, F.; Trianni, G. Rapid damage detection in the Bam area using multitemporal SAR and exploiting ancillary data. *IEEE Trans. Geosci. Remote Sens.* **2007**, *45*, 1582–1589. [[CrossRef](#)]
11. Sato, M.; Chen, S.W.; Satake, M. Polarimetric SAR analysis of tsunami damage following the March 11, 2011 East Japan earthquake. *Proc. IEEE* **2012**, *100*, 2861–2875. [[CrossRef](#)]
12. Watanabe, M.; Motohka, T.; Miyagi, Y.; Yonezawa, C.; Shimada, M. Analysis of urban areas affected by the 2011 off the Pacific Coast of Tohoku earthquake and tsunami with L-band SAR full-polarimetric mode. *IEEE Geosci. Remote Sens. Lett.* **2012**, *9*, 472–476. [[CrossRef](#)]
13. Balz, T.; Liao, M. Building-damage detection using post-seismic high-resolution SAR satellite data. *Int. J. Remote Sens.* **2010**, *31*, 3369–3391. [[CrossRef](#)]
14. Dell’Acqua, F.; Gamba, P.; Polli, D.A. Earthquake damage assessment from post-event VHR radar data: From Sichuan, 2008 to Haiti, 2010. In Proceedings of the IEEE Joint Urban Remote Sensing Event (JURSE), Munich, Germany, 11–13 April 2011; pp. 201–204.
15. Polli, D.; Dell’Acqua, F.; Gamba, P.; Lisini, G. Earthquake damage assessment from post-event only radar satellite data. In Proceedings of the Eighth International Workshop on Remote Sensing for Disaster Response, Tokyo, Japan, 30 September–1 October 2010.
16. Chen, S.W.; Sato, M. Tsunami damage investigation of built-up areas using multitemporal spaceborne full polarimetric SAR images. *IEEE Trans. Geosci. Remote Sens.* **2013**, *51*, 1985–1997. [[CrossRef](#)]
17. Guo, H.; Liu, L.; Zhang, L.; Fan, X.; Li, X.; Zhang, L. *Earth Observation for Earthquake Disaster Monitoring and Assessment*; INTECH Open Access Publisher: Rijeka, Croatia, 2012.
18. Li, X.; Guo, H.; Zhang, L.; Xiao, C.; Lei, L. A new approach to collapsed building extraction using RADARSAT-2 polarimetric SAR imagery. *IEEE Geosci. Remote Sens. Lett.* **2012**, *9*, 677–681.
19. Zhao, L.; Yang, J.; Li, P.; Zhang, L.; Shi, L.; Lang, F. Damage assessment in urban areas using post-earthquake airborne PolSAR imagery. *Int. J. Remote Sens.* **2013**, *34*, 8952–8966. [[CrossRef](#)]
20. Shen, J.C.; Xu, X.; Dong, H.; Gui, L.; Song, C. Collapsed building extraction from single full polarimetric SAR image after earthquake. *Sci. Technol. Eng.* **2015**, *15*, 86–91.
21. Lee, J.S.; Schuler, D.L.; Ainsworth, T.L. Polarimetric SAR data compensation for terrain azimuth slope variation. *IEEE Trans. Geosci. Remote Sens.* **2000**, *38*, 2153–2163.

22. Kimura, H.; Papathanassiou, K.P.; Hajns, I. Polarization orientation effects in urban areas on SAR data. In Proceedings of the IEEE International Geoscience and Remote Sensing Symposium, Seoul, Korea, 25–29 July 2005; pp. 4863–4867.
23. Lee, J.S.; Grunes, M.R.; Kwok, R. Classification of multi-look polarimetric SAR imagery based on complex Wishart distribution. *Int. J. Remote Sens.* **1994**, *15*, 2299–2311. [[CrossRef](#)]
24. Rodrigues, A.; Corr, D.G.; Pottier, E.; Ferro-Famil, L. Land cover classification using polarimetric SAR data. In Proceedings of the Workshop on POLinSAR—Applications of SAR Polarimetry and Polarimetric Interferometry, Frascati, Italy, 14–16 January 2003.
25. Yamaguchi, Y.; Moriyama, T.; Ishido, M.; Yamada, H. Four-component scattering model for polarimetric SAR image decomposition. *IEEE Trans. Geosci. Remote Sens.* **2005**, *43*, 1699–1706. [[CrossRef](#)]
26. Yamaguchi, Y.; Yajima, Y.; Yamada, H. A four-component decomposition of POLSAR images based on the coherency matrix. *IEEE Geosci. Remote Sens. Lett.* **2006**, *3*, 292–296. [[CrossRef](#)]
27. China Earthquake Administration. Preliminary Remote Sensing Results of Qinghai Yushu Earthquake Emergency. Available online: [http://www.cea.gov.cn/manage/html/8a8587881632fa5c0116674a018300cf/\\_content/10\\_04/17/1271485532211.html](http://www.cea.gov.cn/manage/html/8a8587881632fa5c0116674a018300cf/_content/10_04/17/1271485532211.html) (accessed on 20 November 2015).
28. Guo, H.D.; Zhang, B.; Lei, L.P.; Zhang, L.; Chen, Y. Spatial distribution and inducement of collapsed buildings in Yushu earthquake based on remote sensing analysis. *Sci. China Earth Sci.* **2010**, *53*, 794–796. [[CrossRef](#)]
29. Ma, X.; Shen, H.; Zhang, L.; Yang, J.; Zhang, H. Adaptive anisotropic diffusion method for polarimetric SAR speckle filtering. *IEEE J. Sel. Topics Appl. Earth Observ. Remote Sens.* **2015**, *8*, 1041–1050. [[CrossRef](#)]
30. Ma, X.; Shen, H.; Yang, J.; Zhang, L.; Li, P. Polarimetric-spatial classification of SAR images based on the fusion of multiple classifiers. *IEEE J. Sel. Topics Appl. Earth Observ. Remote Sens.* **2014**, *7*, 961–971.
31. Samat, A.; Du, P.; Baig, M.H.A.; Sumit, C.; Liang, C. Ensemble learning with multiple classifiers and polarimetric features for polarized SAR image classification. *Photogramm. Eng. Remote Sens.* **2014**, *80*, 239–251. [[CrossRef](#)]



© 2016 by the authors; licensee MDPI, Basel, Switzerland. This article is an open access article distributed under the terms and conditions of the Creative Commons by Attribution (CC-BY) license (<http://creativecommons.org/licenses/by/4.0/>).